RSC Sustainability

ROYAL SOCIETY OF CHEMISTRY

PAPER

View Article Online
View Journal | View Issue

Cite this: *RSC Sustainability*, 2025, **3**, 1741

An aqua regia-free chemical recovery and reprecipitation of Ir from IrO_x catalysts: optimisation of the extraction efficiency using surface response methodology†

Sarah Turnbull,‡ Delphine Clauss, ‡* Vincent Martin, Jean-Pierre Magnin, Laetitia Dubau and Frédéric Maillard *

Received 17th January 2025
Accepted 1st March 2025

DOI: 10.1039/d5su00038f

rsc.li/rscsus

The widespread deployment of hydrogen is essential in the energy transition away from fossil fuels. There is an increasing demand for iridium (Ir) in the proton-exchange membrane water electrolysis (PEMWE) industry, acting as the catalyst for the oxygen evolution reaction (OER). However, Ir is one of the rarest platinum group metals (PGMs) and its recycling requires significant energy and has considerable environmental impacts. Therefore, developing an innovative energy-efficient recycling method is essential to enhance the use of Ir. This study focuses on the development of a microwave-assisted leaching protocol of Ir from a commercial iridium oxide (IrO_x) catalyst and its reprecipitation in the form of a salt. A Box–Behnken optimisation of the Ir leaching efficiency was performed by varying the temperature (70–200 °C), chloride concentration ($[Cl^-]$) (0–4 M) and hydrogen peroxide concentration ($[H_2O_2]$) (0–3% v/v). An optimum of 91% extraction efficiency was predicted and then confirmed experimentally, achieving an Ir leaching efficiency of 83 ± 10%, which corresponds to an Ir mass extraction of 769 $mg_{Ir}\ g_{IrO_x}^{-1}$. The precipitation of the Ir leachate solution was then performed to obtain Ir in the form of ammonium hexachloroiridate ($(NH_4)_2IrCl_6$) with 94.6% purity.

Sustainability spotlight

The transition to hydrogen energy demands increased use of iridium (Ir) for proton-exchange membrane water electrolysis (PEMWE) catalysts. However, Ir is one of the rarest platinum-group metals, with its extraction and recycling posing significant environmental and energy challenges. This study introduces an energy-efficient leaching method to enhance Ir recycling efficiency, achieving an 83 ± 10% Ir recovery with minimal energy consumption. Such innovation aligns with Sustainable Development Goal #12 of the United Nations and is crucial for sustainable Ir use in PEMWE devices.

Introduction

Iridium (Ir) is one of the rarest earth elements, with a natural abundance of 0.02 ng g^{-1} and a global production of less than ten tons a year.[1] This precious metal is valued due to its high corrosion resistance, high melting point and high density, which makes it a valuable component for high temperature applications such as spark plugs, hydrogenation catalysts, steam reforming catalysts, tail gas purification, and electroluminescence.[2–4] Various studies have also demonstrated the biocompatibility of IrO_x nanoparticles (NPs), and the use of IrO_2 NPs for medical applications is under study.[4] Finally, iridium oxides IrO_2/IrO_x are used as state-of-the-art electrocatalysts for the oxygen evolution reaction (OER) at the anode in proton-exchange membrane water electrolysers (PEMWEs), facilitating the production of green hydrogen (H_2).[5–7] According to the Johnson Matthey Pt-group metal (PGM) Market Report of May 2023, the global annual demand in 2023 for Ir was estimated to be 7.4 tons, with 3.3 tons coming only from the electrochemical industry.[8] The limited supply of Ir and its growing demand highlight the necessity to develop efficient recycling processes from end-of-life (EoL) materials. According to Minke *et al.*, the technical EoL recycling rates for Ir catalysts must reach a minimum of 90% to cover future Ir demand for the large-scale industrialisation of PEMWE devices.[9]

Hydrometallurgy is a well-researched method for the recovery of PGMs. It has an environmental advantage over pyrometallurgy due to its low process temperatures whilst maintaining high metal recovery values. A hydrometallurgical method is based on three key steps: (1) leaching the metal in

Univ. Grenoble Alpes, Univ. Savoie-Mont-Blanc, CNRS, Grenoble-INP, LEPMI, 38000 Grenoble, France. E-mail: frederic.maillard@grenoble-inp.fr; delphine.clauss@grenoble-inp.fr

† Electronic supplementary information (ESI) available. See DOI: https://doi.org/10.1039/d5su00038f

‡ These two authors contributed equally.

appropriate aqueous media (alkaline or acidic) with the addition of different reagents (*e.g.* hydrogen peroxide (H_2O_2) to oxidize the metal atoms to an ionic form, hydrofluoric acid (HF) or sodium chloride (NaCl) to increase the complexing action);[10–12] (2) concentrating and purifying the metal in solution; (3) recovering the metal in pure form or as a salt.[13] The leaching step is often the limiting process, especially for metals such as Ir, whose stability range encompasses most of the water domain at 25 °C, in the absence of a complexing agent.[14] Aqua regia (HCl + HNO_3) remains the preferred solution to leach PGMs, despite high corrosivity.[15] Other used leaching methods combine a high concentration of HCl and an oxidising agent such as hydrogen peroxide (H_2O_2)[22] or sodium chlorate ($NaClO_3$).[23]

However, metallic Ir is highly resistant to most acids and oxidizing agents, making hydrometallurgical methods largely ineffective for its dissolution. Instead, techniques such as alkaline fusion, molten salt chlorination, or alloy fragmentation have demonstrated high dissolution rates. The core principle behind these methods is to convert metallic Ir into a compound that can easily be dissolved. A summary of the methods existing to leach Ir is presented in Table 1 and the interested reader is referred to two recent review articles discussing the topic.[20,24] Yoshimura *et al.*[21] proposed an innovative approach using "dry aqua regia" (a mixture of $FeCl_3$ and KCl), where Ir dissolves as Ir^{3+} ions. They achieved Ir recovery ratios of 28.3% and 45.7% through treatment with HNO_3 and H_2O_2, respectively. Similar methods employing HCl–NaCl–H_2O_2 systems have also been utilized to extract Pt and other PGMs.[25–27] Melke *et al.* introduced a method to recover PGMs from Membrane Electrode Assemblies (MEAs) used in PEMWEs.[17] Their process involves separating the membrane from the catalyst layers, melting the resulting solid powder with sodium peroxide (Na_2O_2) at 550 °C to convert the metals into water-soluble complexes, and subsequently dissolving them in diluted hydrochloric acid (HCl). Each metal is then separated individually.

Notably, all these methods require the use of concentrated acids and significant quantities of chemicals. These processes have substantial environmental impacts due to high energy consumption, extensive chemical use, and the emission of harmful gases (*e.g.*, Cl_2 and N_2O). Moreover, it is important to keep in mind that all the studies presented here are applied to the leaching of metallic Ir. To the best of our knowledge, there is no specific method developed to recover Ir from its oxides, especially as NPs.[4] Therefore, there is a pressing need to develop a more environmentally friendly IrO_x leaching process.

In this study, we describe the development of an environmentally friendly Ir leaching process from iridium oxides (IrO_x), designed to minimize environmental impact. Our approach avoids the use of aggressive reagents and operates under milder conditions compared to conventional hydrometallurgical methods. This was achieved by developing a microwave-assisted protocol for leaching commercial iridium oxide dihydrate ($IrO_2 \cdot 2H_2O$) without the use of aqua regia, employing low acid concentrations and moderate temperatures. The leaching parameters were optimized through a systematic approach, beginning with a screening design followed by a Box–Behnken optimization design to identify the most influential factors and maximize Ir extraction efficiency. Following leaching, Ir ions were reprecipitated as a salt, concentrating them in solid form to facilitate recovery. This study represents a significant advancement in reducing energy consumption and reagent use while maintaining high efficiency in the Ir recovery processes.

Results and discussion

A commercial iridium oxide dihydrate catalyst (99.99%, Ir 73% min., Thermo Scientific Chemicals), referred to as IrO_x hereafter, was the starting material for all experiments performed in this work. Transmission electron microscopy (TEM) images, X-ray diffractograms (XRD) and X-ray photoelectron spectra (XPS) of this material are presented in Fig. S1.† X-ray diffraction reveals the presence of a metallic phase, but no Ir(0) is detected from the XPS fit, suggesting an Ir-core@IrO_x-shell structure in which metallic Ir is located in the core of the particles (XPS being a surface sensitive technique) and is coated with a poorly crystalline IrO_x shell. From the Scherrer equation, the crystallite size of the metallic fraction can be estimated to be 44 nm. Morphological heterogeneity poses a challenge for the Ir leaching process as the lixiviation proceeds on the surface of the IrO_x particles: larger particles are likely to dissolve more slowly than smaller ones. Chemical heterogeneity is a challenge, as the

Table 1 Table summarizing methods reported in the literature for the leaching of metallic Ir

Techniques	Starting material	T [°C]	Time [h]	Chemicals used	Possible hazards	Yield	Ref.
Alkaline fusion/melt acid leaching	Metallic Ir	600	4	Na_2O_2 and HCl 3 M	Production of Cl_2 Na_2O_2 is corrosive and toxic by inhalation	100%	16 and 17
Molten salt chlorination	Metallic Ir	625	2	NaCl, Cl_2, and aqua regia (HCl + HNO_3)	Production of Cl_2 and N_2O Use of concentrated acids	80%	18
Alloy fragmentation	Metallic Ir	1300	1	$CaCO_3$, HCl	Production of Cl_2	100%	19
Alloy fragmentation	Metallic Ir	800–1500	0.2–11	Zn, Sn, Al, Ni, Cu, Mn, aqua regia or HCl + Cl_2	Use/Production of Cl_2 Alloys may be thermally unstable and ignite or explode	70–100%	20
Dry aqua regia	Metallic Ir	350–400	2–8	$FeCl_3$, HCl, HNO_3, and H_2O_2	Production of Cl_2 and N_2O	45.7%	21

method developed will need to be able to dissolve Ir in various degrees of oxidation.

The Ir dissolution reaction can be summarised in eqn (1), while the standard potential *vs.* the standard hydrogen electrode (SHE) of the redox couples are given in eqn (2) and (3).[28] These equations show that the presence of chloride (Cl^-) ions weakens the metallic bonds by enabling the formation of a stable complex ($IrCl_6^{2-}$).[29]

$$IrO_2 + 4H^+ + 6Cl^- \rightarrow IrCl_6^{2-} + 2H_2O \quad (1)$$

$$IrO_2 + 4H^+ + 4e^- = Ir + 2H_2O \; E^\circ = 0.926\ V_{SHE} \quad (2)$$

$$IrCl_6^{2-} + 4e^- = Ir + 6Cl^- \; E^\circ = 0.860\ V_{SHE} \quad (3)$$

The Gibbs free energy of eqn (1) calculated using the standard potentials of reactions eqn (2) and (3) is negative ($\Delta G^\circ = -0.025$ kJ mol^{-1}), indicating that it is spontaneous. However, thermodynamic feasibility does not guarantee fast Ir dissolution kinetics and preliminary leaching experiments at $T = 40$ °C for 24 hours in both acidic and alkaline media demonstrated limited Ir extraction efficiency. To accelerate the Ir dissolution kinetics, we used microwave heating. Microwave-assisted leaching has been used in previous studies for the recovery of PGMs from catalyst materials.[30,31] It is a highly efficient route as shown by Suoranta *et al.*, who achieved a rhodium leaching efficiency of 79 ± 3% with microwave assisted leaching, compared to just 20 ± 1% with conventional heating.[31]

In this study, a microwave oven and polytetrafluoroethylene (PTFE) reactors were used to elevate the temperature and pressure of the solution, thereby kinetically favouring the production of $IrCl_6^{2-}$. Details of the reactor vessels and conditions are provided in the ESI.† Due to experimental limitations of the Mars 6™ CEM microwave oven used, namely the propensity of the sapphire thermowell to leach at alkaline pH, acidic conditions were chosen for the lixiviation. Moreover, acidic conditions allow for ultraviolet-visible (UV-vis) titration of Ir in solution as $IrCl_6^{2-}$. Indeed, Zhao *et al.*[32,33] demonstrated that in a high pH solution, $IrCl_6^{2-}$ undergoes hydrolysis, where the chloride ligands are exchanged for hydroxide ligands, forming $Ir(OH)_6^{2-}$, which is colourless (eqn (4)). Massué *et al.* suggested that the discolouration is attributed to the disappearance of strong ligands to metal charge transfer (LMCT) bands.[34] Therefore, it is important that the solutions are maintained at a low pH to accurately quantify Ir using UV-vis. The UV-vis spectrum displayed in Fig. S2a† is comparable to the literature.[35]

$$IrCl_6^{2-} + 6OH^- \rightarrow Ir(OH)_6^{2-} + 6Cl^- \quad (4)$$

The $IrCl_6^{2-}$ species exhibits most intensity in the region 600–400 nm with four distinctive peaks at $\lambda = 488$ nm (x), 434 nm (y), 418 nm (z), and 305 nm (w). $H_2IrCl_6 \cdot xH_2O$ (99.9% trace metals basis, Merck) was used to make up standard solutions of Ir in a concentration range of 50–250 ppm. Linear plots of the absorbance at wavelengths x, y, z, and w against the concentration of Ir are displayed in the ESI (Fig. S2b).† Each line passes through the origin with an adjusted R-squared value >0.99 (Table S2†). The Beer–Lambert law states that the absorbance of light by a sample (A) is directly proportional to the concentration of the species in the sample (c) and the path length (l) through which the light passes. The molar extinction coefficient (ε/dm^3 mol^{-1} cm^{-1}) is determined from the slope of the line in the absorbance *vs.* concentration graph. The molar extinction coefficient values of the complex displayed in Table S2† are in the same order of magnitude as those in the literature.[35] The bands represent LMCT whereby the partially filled low-lying t_{2g} and e_g* molecular orbitals (MOs) of the Ir^{4+} cations accept electrons from the σ- and π-bonding MOs of the chloride ligands. The equation of the line at wavelength 488 nm was used to calculate the Ir concentration (C_{Ir}/mol L^{-1}) in the leachate as detailed in eqn (5), where A is the absorbance of the solution at 488 nm and 3897.7 (L mol^{-1}) corresponds to the slope (which corresponds to εl in the Beer–Lambert law) of the calibration curves of the absorbance against the concentration of Ir in $H_2IrCl_6 \cdot xH_2O$ in standard solutions for $\lambda = 488$ nm (see Fig. S2b and Table S2†). The peak at this wavelength displays the highest absorbance intensity and is well-separated from other peaks. The maximum possible concentration of Ir in solution ($C_{Ir(max)}$/mol L^{-1}) was calculated from eqn (6) where m_{IrO_x} is the initial mass of commercial IrO_x, 0.7361 is the fractional weight of Ir in IrO_x provided by the manufacturer, M_{Ir}/g mol^{-1} is the molar mass of Ir, and V_L/L is the volume of the leachate. Finally, the percent extraction was calculated using eqn (7).

$$C_{Ir} = \frac{A}{3897.7} \quad (5)$$

$$C_{Ir(max)} = \frac{m_{IrO_x} \times 0.7361}{M_{Ir}} \times \frac{1}{V_L} \quad (6)$$

$$\text{Extraction}(\%) = \frac{C_{Ir}}{C_{Ir(max)}} \times 100 \quad (7)$$

To first screen through multiple experimental factors (temperature, solid-to-liquid ratio (S/L), $[H_2O_2]$, $[H^+]$ and $[Cl^-]$) and determine those that are critical and those that are less significant towards the extraction efficiency of Ir in the leaching process, a two-level factorial design using Stat-Ease 360® was conducted. Factorial designs are statistical experimental designs that offer the ability to investigate the effects and the interactions of two or more independent factors. By manipulating the levels of the factors and measuring the resulting impact on the dependent variables, the main effects can be identified. Moreover, factorial designs allow a study of multiple factors simultaneously, reducing the number of experiments required as opposed to testing each factor separately. The ranges of each factor were chosen with careful consideration based on the results of preliminary experiments and what was experimentally achievable. Note that the factor range may affect the validity and interpretability of the results. For example, if the range is too narrow for a given factor, the study may fail to capture the full range in which the response occurs. On the other hand, a range too broad may infer practical restraints and a loss of precision where the response occurs.

Sulfuric acid (H_2SO_4) was selected to provide protons, and a range of 0.5 to 4.0 M for $[H_2SO_4]$ was chosen. NaCl was used as a chloride source without further increasing the acidity of the leachate solution. $[H^+]$ and $[Cl^-]$ were chosen as separate factors to distinguish if one was more significant than the other and to investigate if it was possible to optimize the leaching process while retaining mild acidity. The upper limit of the S/L ratio was set at 0.25 g L^{-1}, while the lower limit for the S/L factor was set at 0.1 g L^{-1}. Due to experimental limitations (maximum mass of 2.5 mg in 10 mL in the reaction vessel) and practical restraints (increased error when weighing <2.5 mg), a broader range of S/L values and their effect on the Ir extraction efficiency could not be fully investigated. The T values were chosen within a range of 70 to 200 °C. The Mars 6™ CEM microwave handbook recommends the introduction of a second ramp at temperatures above 200 °C. To be consistent with the hold time, t of the reaction and avoid extreme temperatures and possible distortion of the vessels, 200 °C was chosen as the upper limit. Finally, H_2O_2 is an oxidising agent often used to aid the extraction of PGMs into solution.[15,27,36] It undergoes reduction into various species as shown in eqn (8)–(10),[37] aiding in the oxidation of metal species by accepting their electrons. For example, Kazemi *et al.*[36] reported higher platinum extraction with the addition of 3% v/v H_2O_2 in the leach solution according to eqn (11).

$$H_2O_2 + 2H^+ + 2e^- = 2H_2O \; E^\circ = 1.35 \; V_{SHE} \quad (8)$$

$$H_2O_2 + H^+ + e^- = HO^\bullet + H_2O \; E^\circ = 0.39 \; V_{SHE} \quad (9)$$

$$HO^\bullet + H^+ + e^- = H_2O \; E^\circ = 2.31 \; V_{SHE} \quad (10)$$

$$Pt + 2H^+ + 4Cl^- + H_2O_2 \rightarrow PtCl_4^{2-} + 2H_2O \quad (11)$$

Therefore, the concentration of H_2O_2 was considered an important factor to be tested for the Ir extraction efficiency. For safety reasons, a maximum concentration of 3% v/v H_2O_2 was selected. Higher concentrations would raise the risk of explosive H_2O_2 decomposition, facilitating degassing of the PTFE vessels. The absence of H_2O_2 (0% v/v) was chosen as the lower limit to test the full effect of this factor. Finally, before applying the surface design plan, the reaction time was set to 30 min. The kinetics of the reaction was then studied using the optimized parameters, as presented in the following.

Table S3† displays the chosen factors and their ranges for the factorial design in order to screen factors of least impact on the Ir extraction efficiency. Table S4† displays the design plan and the response values for the extraction efficiency of Ir. The experimental results were analysed with Design Expert software and models were refined by eliminating statistically insignificant model terms, except for those required to support hierarchy. The p-value probability was used to identify significance for each term. If the p-value is less than 0.05 then the terms are significant for the model, and those between 0.05 and 0.1 were manually evaluated. All effects for models, simple, interaction, and quadratic terms, showed a p-value of less than 0.05, indicating that models were significant and represented the area of study. The suitability and adequacy of both models were measured using ANOVA factors and are summarized in Table S5.† Analyses were carried out with a significance level of 0.05. This value represents a 5% risk of incorrectly concluding that a difference exists when, in reality, no such difference is present. No transformation for the Y response was required to ensure that the model meets the assumptions required for the analysis of variance (ANOVA). Statistical factors were acceptable, as shown in Table S6.† The lack of fit (LOF) (p-value > 0.1) was not significant which implied good quality of the model correlation between the process variables and the responses. The multiple correlation coefficient adjusted R-squared superior to 0.85 and its closeness to predicted R-squared confirmed the accuracy of the models. The coefficient of variation (CV), an indicator of the degree of precision, up to 10% means that the model has good accuracy. To complete this analysis, studying the residuals (= predicted response values − experimental values) is crucial to understanding their behaviour. It mainly concerns 3 points which must be verified:

(1) The residuals follow a normal distribution, because the experimental error must follow a normal distribution; (2) the residuals are independent of the response, because the variance of the experimental error must be constant and thus independent of the response; (3) the residuals are independent of the order of the experiments, because the variance of the experimental error must be constant and thus independent of the answer.

All diagnostic tests were satisfactory, implying that the models were acceptable for optimization and validation. The final model relationship between the response (Ir extraction efficiency) and the continuous factors, after the refining step, was described by a second order polynomial (eqn (12)).

$$\sqrt{\text{Ir extraction}} = -2.51 - 1.15 \times \frac{S}{L} + 3.11 \times [H^+] + 3.33 \times [Cl^-] + 9.04E-03 \times T + 0.02 \times \frac{S}{L} \times T - 1.31 \times [H^+] \times [Cl^-] \quad (12)$$

From the screening phase, it can be safely concluded that the temperature and $[Cl^-]$ have a positive effect on the leaching process (Table S5†). Interestingly, while an increase in $[H^+]$ should theoretically shift the equilibrium of (eqn (1)) to the right, the ANOVA results from the factorial design indicate that $[H^+]$ is not as significant a factor compared to others in determining extraction dissolution efficiency. Therefore, $[H^+]$ was set to 0.5 M for the optimization process. Moreover, there seems to be a negative effect of increasing the S/L ratio on the Ir extraction efficiency, which can be attributed to the higher mass of the IrO_x starting material within the same liquid volume, leading to reduced dispersion of solid particles in the solution. Nevertheless, the interactions between S/L and H_2O_2, as well as temperature and H_2O_2, also demonstrate a positive effect. During the optimization step, an S/L ratio of 0.25 g L^{-1} was selected, following the vessel recommendations.

Three factors were chosen, namely, T, $[Cl^-]$ and $[H_2O_2]$, to optimize the Ir extraction efficiency. To optimise multiple

Table 2 Experimental factors and levels for the Box–Behnken design used for optimising the Ir extraction efficiency from IrO_x under microwave conditions

		Level		
Factor	Unit	−1	0	1
$[Cl^-]$	M	0	1	2
Temperature	°C	70	135	200
$[H_2O_2]$	%v/v	0	1.5	3

factors for a desired response, surface design plans can be utilised. The most common methods include Central Composite designs (CCDs), Box–Behnken designs (BBD), and optimal designs.[38] BBD was chosen as it requires fewer experimental runs.[36] This method has already been utilized to optimize the recovery of Pt by Ding *et al.*[27] BBDs have three levels for each factor and are built to fit a quadratic model. The model works best using a small range of the chosen factors and gives high prediction precision in the centre of the factor space. The accuracy of the input is critical for the dependability of the model. The chosen ranges of factors (T, $[Cl^-]$ and $[H_2O_2]$) are displayed in Table 2 and were based on preliminary experiments and the screening phase in which an optimum of the Ir extraction efficiency was expected. Table 3 displays the experimental plan and the responses that were used for the Box–Behnken optimisation model. 3-Dimensional Box–Behnken optimisation models for the Ir extraction efficiency are

Table 3 Design plan and responses for the Box–Behnken optimisation of Ir extraction efficiency for factors at given levels under microwave conditions. Reaction hold t = 30 min, S/L = 0.25 g L^{-1}, $[H^+]$ = 0.5 M

Run	Temperature (°C)	$[Cl^-]$ (M)	$[H_2O_2]$ (M)	Response in Ir extraction efficiency (%)	Response in Ir mass extraction ($mg_{Ir}\ g_{IrO_x}^{-1}$)
1	135	2	0	35	254
2	135	1	1.5	19	137
3	200	1	0	9	63
4	70	0	1.5	0	0
5	135	0	0	0	0
6	135	1	1.5	41	302
7	200	1	3	91	109
8	70	1	3	15	666
9	70	1	0	5	34
10	70	2	1.5	9	64
11	135	1	1.5	24	173
12	200	0	1.5	0	0
13	135	0	3	0	0
14	200	2	1.5	11	84
15	135	1	1.5	24	172
16	135	1	1.5	27	198

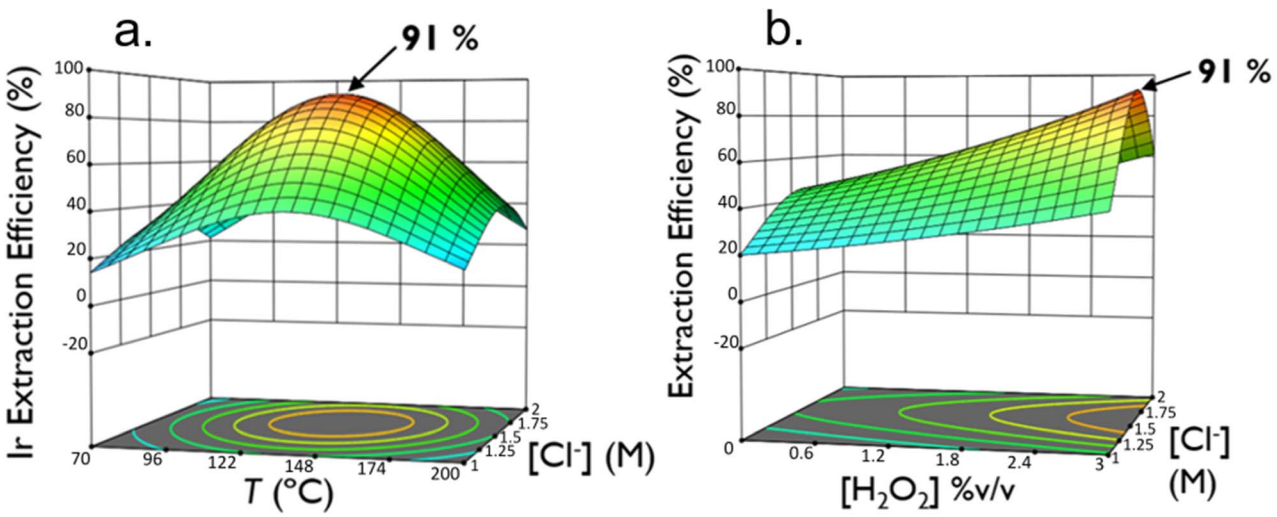

Fig. 1 (a) Side view of the optimisation model for the Ir extraction efficiency as a function of $[Cl^-]$ and temperature. $[H_2O_2]$ = 3% v/v, S/L ratio = 0.25 g L^{-1}. (b) Side view of the optimisation model for the Ir extraction efficiency as a function of $[Cl^-]$ and $[H_2O_2]$. T = 135 °C and S/L ratio = 0.25 g L^{-1}. Graduated coloured areas from cool blue for lower response levels to red for higher values are presented in 3D graphs. Blue and red areas represent the 25% and 75% ranges of the maximal value obtained in the representation, respectively.

displayed in Fig. 1. Fig. 1b clearly shows that an increase in $[H_2O_2]$ enhances the dissolution in Ir. However, there is insufficient evidence to determine an optimum $[H_2O_2]$ for the Ir extraction efficiency under these conditions. While it appears that further increasing the $[H_2O_2]$ beyond 3% v/v could improve the Ir extraction efficiency, the concentration was only tested up to 3% v/v due to the explosive risks associated with the decomposition of H_2O_2 into molecular oxygen and water.

A striking result in Table 3 is the fundamental role played by $[Cl^-]$, as we observe an Ir extraction efficiency of 0% in each run where $[Cl^-] = 0$ M. According to Fig. 1a, there is an optimum in $[Cl^-]$ for the extraction efficiency of Ir at $[Cl^-] = 1.6$ M at $T = 139$ °C and $[H_2O_2] = 3\%$ v/v. The increase in extraction efficiency up to $[Cl^-]$ of 1.6 M can be explained by the shifting of the equilibrium to the right in eqn (1) according to Le Chatelier's principle. Above 1.6 M, the decrease in extraction efficiency can be explained by the evolution of chlorine (Cl_2) gas from the oxidation of Cl^- ions (eqn (13)).[39] Although Cl_2 evolution was not confirmed (as it was not investigated in this study), the release of Cl_2 gas from the reaction vessel could reduce the Cl^- concentration in solution, leading to a decrease in Ir extraction efficiency due to less reagent being available for the formation of $IrCl_6^{2-}$. Further investigations, such as implementing the measure of the Cl_2 concentration during the leaching, should be investigated to confirm this hypothesis.

$$2Cl^- \rightarrow Cl_{2(g)} + 2e^- \quad (13)$$

From the optimisation model of the Ir extraction efficiency as a function of temperature and $[Cl^-]$ (Fig. 1a), there is also an optimum in the temperature at 139 °C. The increase in Ir extraction efficiency up to 139 °C can be explained by the increase in the rate constant for the reaction according to Arrhenius' law. The decrease in extraction efficiency at temperatures above 139 °C can be explained by the competition of other reactions, namely, the evolution of Cl_2 and the decomposition of H_2O_2, thereby decreasing the concentration of complexing and oxidising agent in solution, respectively. Indeed, it is well-established that increasing the temperature accelerates the decomposition rate of H_2O_2 (see eqn (8) and (9)).[40,41] It has also been demonstrated that Ir, under oxidative conditions, can catalyse the evolution of Cl_2 [42,43] and that increasing temperature enhances the reaction rate. However, this is a hypothesis and further research studies need to be conducted to better understand the temperature maximum point.

Confirmation of the optimisation model is usually done at or near the numerical optimisation. Therefore, microwave leaching conditions of $T = 139$ °C, $[Cl^-] = 1.6$ M, and $[H_2O_2] = 3\%$ v/v were selected with constant values for $[H^+] = 0.5$ M, S/L = 0.25 g L^{-1}, and hold time $t = 30$ min. These conditions resulted in an Ir extraction efficiency of 83 ± 10% which falls in the range for the system model statistics in the ESI (Table S7).† This corresponds to an Ir mass extraction of 769 mg_{Ir} $g_{IrO_x}^{-1}$. To determine the kinetics of the Ir dissolution reaction under microwave conditions and confirm the chosen reaction time, reactions were performed altering the hold t of the reaction. The results are displayed in Table 4. The concentration of Ir in solution against the hold t of the reaction is shown in Fig. 2.

Each experiment involved a ramp t of 20 min to the desired temperature. Increasing the hold t of the reaction from 0 to 30 min results in greater Ir extraction efficiency. However, beyond 30 min, the increase in Ir extraction efficiency was not statistically significant. This indicates that performing these leaching experiments for longer than 30 min is unnecessary. By limiting the hold time t to a maximum of 30 min, it is possible to limit the energy consumption linked to Ir leaching. The observed plateau in the leaching efficiency after 30 min could be associated with the deactivation of the leachate during the experiment

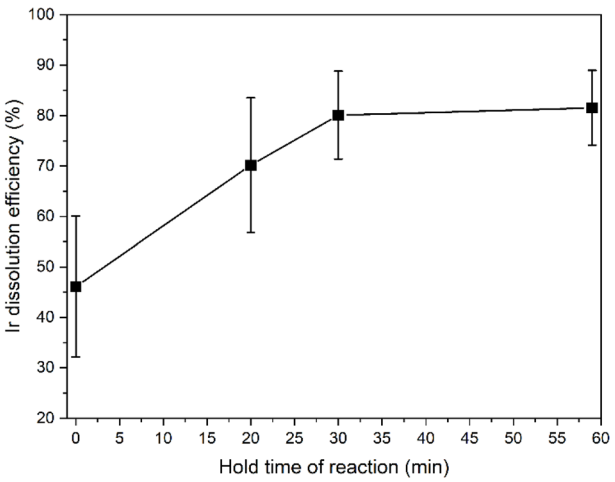

Fig. 2 Kinetic model of the extraction of Ir into solution at various holding times. $T = 139$ °C, $[Cl^-] = 1.6$ M, $[H_2O_2] = 3\%$ v/v, S/L = 0.25 g L^{-1}. The measurements were conducted three times, and the average results are presented, with error bars representing the standard deviation of the three replicates.

Table 4 Ir dissolution in microwave-assisted leaching experiments, where the holding time at the desired temperature was investigated. The conditions were $T = 139$ °C, $[Cl^-] = 1.6$ M, $[H_2O_2] = 3\%$ v/v, S/L = 0.25 g L^{-1} and ramp time = 20 min

Hold time (min)	Absorbance at 488 nm	Concentration of Ir ($\times 10^{-4}$ M)	Max. Ir concentration ($\times 10^{-4}$ M)	Ir extraction efficiency (%)
0	1.7 ± 0.4	4.4 ± 1.3	9.6 ± 0.2	46 ± 14
20	2.6 ± 0.4	6.7 ± 1.3	9.6 ± 0.2	70 ± 13
30	3.0 ± 0.2	7.7 ± 0.8	9.6 ± 0.2	80 ± 9
59	3.0 ± 0.2	7.8 ± 0.7	9.6 ± 0.2	82 ± 7

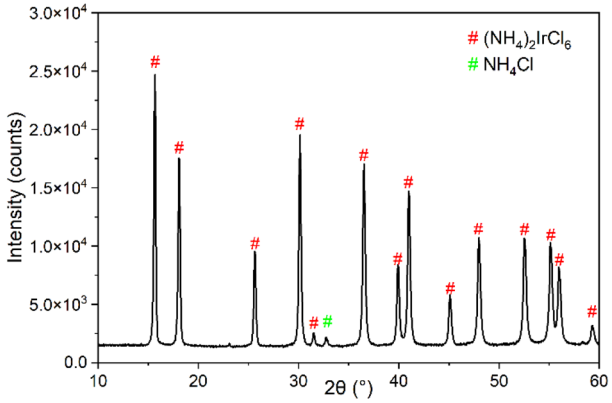

Fig. 3 X-ray diffraction pattern of the recovered precipitate $(NH_4)_2IrCl_6$.

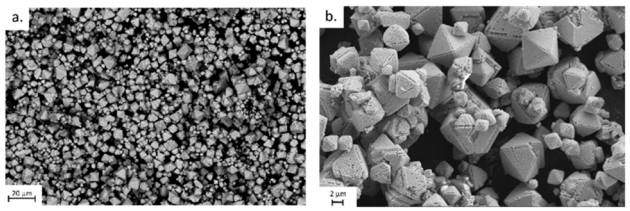

Fig. 4 Scanning electron microscopy images of the $(NH_4)_2IrCl_6$ sample precipitate, magnified (a) 500 and (b) 2k times.

(through H_2O_2 decomposition and Cl_2 evolution). This could also be explained by the presence of metallic Ir in the sample.

Finally, after being extracted into the aqueous phase, Ir was precipitated in the form of a salt by the addition of NH_4Cl and filtered out of solution, following the protocol introduced by Yoshimura *et al.*[21] The reaction scheme is summarised in eqn (14) where $(NH_4)_2IrCl_6$ is the formed precipitate. An $IrCl_6^{2-}$ containing solution obtained from the leaching step under optimum conditions ($T = 139$ °C, $[Cl^-] = 1.6$ M, $[H_2O_2] = 3\%$ v/v, $[H^+] = 0.5$ M, S/L = 0.25 g L^{-1}, and $t = 30$ min) was used as the starting material. The leachate was reacted with NH_4Cl at the highest concentration possible without saturating the solution. This approach was used to shift the equilibrium in eqn (14) to the right, maximizing the formation of the desired precipitate while avoiding the introduction of undissolved NH_4Cl impurities.

$$2[NH_4]_{(aq)}^{+} + IrCl_{6(aq)}^{2-} \rightarrow (NH_4)_2IrCl_{6(s)} \quad (14)$$

Fig. S3† displays the process of the precipitation of $(NH_4)_2IrCl_6$ salt. The change in colour of the solution from deep orange to clear confirms the decrease in the $IrCl_6^{2-}$ concentration in solution and the transfer of Ir into the solid phase. The obtained precipitate was analysed by XRD as shown in Fig. 3 and the pattern was compared to that of Reig-i-Plessis *et al.* and Yoshimura *et al.* who analysed the same crystal structure.[21,44] The Bragg peak positions of $(NH_4)_2IrCl_6$ and NH_4Cl were indicated with markers from the expected patterns of $(NH_4)_2IrCl_6$ and NH_4Cl taken from the International Crystal Structure Database (ICSD).[45] An NH_4Cl minor phase is present because the product was not washed after filtration in order to prevent re-dissolving $(NH_4)_2IrCl_6$; therefore NH_4Cl may have recrystallised out of solution and remained on the filter paper. The main phase is $(NH_4)_2IrCl_6$ with 94.6% purity. Finally, the product was analysed by scanning electron microscopy coupled with energy dispersive X-ray spectroscopy (SEM-EDS). Fig. 4 displays the octahedral crystal structure of $(NH_4)_2IrCl_6$. The energy-dispersive spectrum displayed in Fig. S4† confirms the absence of other impurities in the precipitate sample. The atomic ratios of Ir, Cl and nitrogen (N) were determined from the normal mass as determined using the area under the peaks (Ir, 12 at%; Cl, 69 at%; N, 19 at%). The approximate 1 : 6 ratio of atomic Ir to Cl and 1 : 2 atomic ratio of Ir to N also confirm the presence of $(NH_4)_2IrCl_6$.

In summary, we presented a novel method for leaching IrO_x NPs using microwave-assisted heating in the presence of Cl^- under acidic and oxidative conditions. Our results demonstrate that this approach achieves satisfactory Ir leaching efficiency under milder conditions compared to those reported in the literature for metallic Ir leaching. Table 5 summarizes the key properties of this method using the same criteria as those in Table 1, allowing for a direct comparison with previously reported methods. To ensure a fair comparison between the IrO_x leaching methods, a life cycle assessment of the methods discussed in the literature and the one described here should be implemented, but this falls outside the scope of this work. Importantly, our method operates at significantly lower temperature (139 °C) than other techniques (>400 °C) and offers a faster protocol, which helps reduce energy consumption. Additionally, the acid concentration used is lower than that in existing processes for Ir (not IrO_x) dissolution. Nevertheless, our method still relies on Cl^- ions, which may lead to Cl_2 production—albeit in lower concentrations than in other methods—as well as H_2O_2, a corrosive chemical. Finally, the authors would like to emphasize that this method was specifically developed for leaching IrO_x particles and has not been optimized for metallic Ir. Further work is ongoing to assess the effects of IrO_x particle size, crystallinity, and speciation (mean Ir oxidation state).

Table 5 Main properties of the IrO_x leaching process described in this work. This allows for a comparison of the other Ir leaching processes described in the literature and summarized in Table 1

Technique	Starting material	T [°C]	Time [h]	Chemicals used	Possible hazards	Yield
Microwave assisted leaching	IrO_x NPs	139 °C	0.5	H_2SO_4 0.5 M, NaCl 1.6 M, and H_2O_2 3% v/v	Potential production of Cl_2 H_2O_2 is corrosive and toxic by inhalation	83 ± 10%

Conclusions

In this study, we introduced a microwave-assisted Ir leaching protocol from commercial $IrO_2 \cdot 2H_2O$ and its precipitation from the aqueous phase to recuperate Ir in the form of a salt $(NH_4)_2IrCl_6$. A Box–Behnken optimisation was conducted using an experimental plan with the following factors: temperature, $[Cl^-]$ and $[H_2O_2]$. An optimum Ir extraction efficiency from IrO_x was predicted from the model at 91% for conditions of $T = 139$ °C, $[Cl^-] = 1.6$ M, $[H_2O_2] = 3\%$ v/v, where $[H^+] = 0.5$ M, hold time $t = 30$ min, and S/L = 0.25 g L^{-1}. The experimental Ir extraction efficiency measured under these conditions was 83 ± 10%, highlighting a good correlation between theory and experiment and demonstrating the possibility to reach a high recovery efficiency of Ir from IrO_x. Furthermore, Ir in the form of $IrCl_6^{2-}$ was precipitated from the solution as $(NH_4)_2IrCl_6$ with a purity of 94.6%, as confirmed by X-ray diffraction and energy-dispersive X-ray spectroscopy combined with scanning electron microscopy. This demonstrates the potential to recover leached Ir in a suitable form for revalorization.

Data availability

Data for this article, including the kinetic model of the extraction of Ir into solution (Fig. 2), X-ray diffraction pattern of the recovered precipitate $(NH_4)_2IrCl_6$ (Fig. 3), X-ray photoelectron spectra (Ir 4f band) and X-ray diffraction pattern of the commercial $IrO_2 \cdot 2H_2O$ catalyst (Fig. S1b and c†), UV-vis spectrum of $IrCl_6^{2-}$ species in HCl after microwave-assisted leaching of $IrO_2 \cdot 2H_2O$, calibration curves of the absorbance against the concentration of Ir in $H_2IrCl_6 \cdot xH_2O$ in standard solutions (Fig. S2a and b†), and energy-dispersive X-ray spectrum of the $(NH_4)_2IrCl_6$ sample precipitate (Fig. S4†) are available at the Open Science Framework at **https://osf.io/wkqzs/files/osfstorage/678a498b206c7757dd282b4d**. Note: the data required to build Fig. 1 are available in Tables 2 and 3.

Author contributions

Sarah Turnbull: investigation; sample collection and analysis; formal analysis; drawing; writing – original draft. Delphine Clauss: conceptualization; sample collection and analysis; supervision; validation; writing – original draft, review & editing. Vincent Martin: sample collection and analysis; investigation; data curation. Jean-Pierre Magnin: conceptualization; methodology; validation. Laetitia Dubau: conceptualization; investigation; validation. Frédéric Maillard: conceptualization; data curation; funding acquisition; supervision; validation; writing – review & editing.

Conflicts of interest

There are no conflicts to declare.

Acknowledgements

This work was supported by the "France 2030" government investment plan managed by the French National Research Agency, under the reference "ANR-22-PEHY-0011", in the frame of the MATHYLDE project.

Notes and references

1 J. Burlakovs, Z. Vincevica-Gaile, M. Krievans, Y. Jani, M. Horttanainen, K.-M. Pehme, E. Dace, R. H. Setyobudi, J. Pilecka, G. Denafas, I. Grinfelde, A. Bhatnagar, V. Rud, V. Rudovica, R. L. Mersky, O. Anne, M. Kriipsalu, R. Ozola-Davidane, T. Tamm and M. Klavins, Platinum Group Elements in Geosphere and Anthroposphere: Interplay among the Global Reserves, Urban Ores, Markets and Circular Economy, *Minerals*, 2020, **10**(6), 558, DOI: **10.3390/min10060558**.

2 A. V. Ermakov and S. S. Naboichenko, Iridium: Production, Consumption, and Prospects, *Russ. J. Non-Ferr. Met.*, 2012, **53**(4), 292–301, DOI: **10.3103/S1067821212040049**.

3 M.-L. Cui, Y.-S. Chen, Q.-F. Xie, D.-P. Yang and M.-Y. Han, Synthesis, Properties and Applications of Noble Metal Iridium Nanomaterials, *Coord. Chem. Rev.*, 2019, **387**, 450–462, DOI: **10.1016/j.ccr.2018.12.008**.

4 J. Quinson, Iridium and IrO_x Nanoparticles: An Overview and Review of Syntheses and Applications, *Adv. Colloid Interface Sci.*, 2022, **303**, 102643, DOI: **10.1016/j.cis.2022.102643**.

5 S. S. Kumar and H. Lim, Recent Advances in Hydrogen Production through Proton Exchange Membrane Water Electrolysis – a Review, *Sustainable Energy Fuels*, 2023, **7**(15), 3560–3583, DOI: **10.1039/D3SE00336A**.

6 M. Carmo, G. P. Keeley, D. Holtz, T. Grube, M. Robinius, M. Müller and D. Stolten, PEM Water Electrolysis: Innovative Approaches towards Catalyst Separation, Recovery and Recycling, *Int. J. Hydrogen Energy*, 2019, **44**(7), 3450–3455, DOI: **10.1016/j.ijhydene.2018.12.030**.

7 M. Bernt, A. Hartig-Weiß, M. F. Tovini, H. A. El-Sayed, C. Schramm, J. Schröter, C. Gebauer and H. A. Gasteiger, Current Challenges in Catalyst Development for PEM Water Electrolyzers, *Chem. Ing. Tech.*, 2020, **92**(1–2), 31–39, DOI: **10.1002/cite.201900101**.

8 J. Murawski, S. B. Scott, R. Rao, K. Rigg, C. Zalitis, J. Stevens, J. Sharman, G. Hinds and I. E. L. Stephens, Benchmarking Stability of Iridium Oxide in Acidic Media under Oxygen Evolution Conditions: A Review: Part II: Investigation of Catalyst Activity and Stability *via* Short Term Testing, *Johnson Matthey Technol. Rev.*, 2024, **68**(1), 147–160, DOI: **10.1595/205651324X17055018154113**.

9 C. Minke, M. Suermann, B. Bensmann and R. Hanke-Rauschenbach, Is Iridium Demand a Potential Bottleneck in the Realization of Large-Scale PEM Water Electrolysis?, *Int. J. Hydrogen Energy*, 2021, **46**(46), 23581–23590, DOI: **10.1016/j.ijhydene.2021.04.174**.

10 C. Liu, S. Sun, X. Zhu and G. Tu, Metals Smelting-Collection Method for Recycling of Platinum Group Metals from Waste Catalysts: A Mini Review, *Waste Manage. Res.*, 2021, **39**(1), 43–52, DOI: **10.1177/0734242X20969795**.

11 Z. Peng, Z. Li, X. Lin, H. Tang, L. Ye, Y. Ma, M. Rao, Y. Zhang, G. Li and T. Jiang, Pyrometallurgical Recovery of Platinum

Group Metals from Spent Catalysts, *JOM*, 2017, **69**(9), 1553–1562, DOI: 10.1007/s11837-017-2450-3.

12 L. Sandig-Predzymirska; T. V. Barreiros; A. Thiere; A. Weigelt; D. Vogt; M. Stelter and A. Charitos Recycling Strategy for the Extraction of PGMs from Spent PEM Electrodes. 2021. Available at: https://recycalyse.eu/wp-content/uploads/Paper-Sandig-Predzymirska-Lesia.pdf (Accessed February 24th, 2025).

13 S. Steinlechner and J. Antrekowitsch, Potential of a Hydrometallurgical Recycling Process for Catalysts to Cover the Demand for Critical Metals, Like PGMs and Cerium, *JOM*, 2015, **67**(2), 406–411, DOI: 10.1007/s11837-014-1263-x.

14 M. Pourbaix, *Atlas of Electrochemical Equilibria in Aqueous Solutions*, National Association of Corrosion Engineers, 1974.

15 M. K. Jha, J. Lee, M. Kim, J. Jeong, B.-S. Kim and V. Kumar, Hydrometallurgical Recovery/Recycling of Platinum by the Leaching of Spent Catalysts: A Review, *Hydrometallurgy*, 2013, **133**, 23–32, DOI: 10.1016/j.hydromet.2012.11.012.

16 J. Lee and Y. Kim, Chemical Dissolution of Iridium Powder Using Alkali Fusion Followed by High-Temperature Leaching, *Mater. Trans.*, 2011, **52**(11), 2067–2070, DOI: 10.2320/matertrans.M2011202.

17 J. Melke, A. Maletzko, E. D. Gomez Villa, A. Bornet, G. K. H. Wiberg, M. Arenz, L. Sandig-Predzymirska, A. Thiere, A. Charitos, M. Stelter, Z. Wang, S. Pitscheider, E. Bertheussen, C. M. Pedersen, S. Finsdóttir, M. S. Kokborg, D. G. Berman, S. Dalvang, S. S. Müller, F. Seidel, N. Seselj, M. Höglinger, S. Kartusch, J. Eder, M. Macherhammer, A. Trattner and C. Kallesøe, Recycalyse – New Sustainable and Recyclable Catalytic Materials for Proton Exchange Membrane Electrolysers, *Chem. Ing. Tech.*, 2024, **96**(1–2), 126–142, DOI: 10.1002/cite.202300143.

18 G. B. Kauffman and R. D. Myers, The Recovery of Iridium from Laboratory Residues, *J. Less-Common Met.*, 1978, **60**(1), P1–P3, DOI: 10.1016/0022-5088(78)90102-9.

19 Y. Kobayashi, S. Yamada and T. Nagai, New Dissolution Process of Iridium to Hydrochloric Acid, in *Rare Metal Technology*, 2019, DOI: 10.1007/978-3-030-05740-4_19.

20 C. Fan, K. Quan, Z. Han, F. Han, Z. Li, J. Liu and X. Liu, Recovery and Purification of Iridium from Secondary Resources: A Review, *J. Sustain. Metal.*, 2023, **9**(3), 909–926, DOI: 10.1007/s40831-023-00697-y.

21 A. Yoshimura, H. Komatsuda and Y. Matsuno, Establishment of a Novel Recycling Process for Iridium Using "Dry Aqua Regia.", *Mater. Trans.*, 2024, **65**(1), 49–53, DOI: 10.2320/matertrans.MT-M2023084.

22 W.-S. Chen, W.-S. Liu and W.-C. Chen, Leaching Efficiency and Kinetics of Platinum from Spent Proton Exchange Membrane Fuel Cells by H_2O_2/HCl, *Metals*, 2023, **13**(6), 1006, DOI: 10.3390/met13061006.

23 J. Xia and A. Ghahreman, Platinum Group Metals Recycling from Spent Automotive Catalysts: Metallurgical Extraction and Recovery Technologies, *Sep. Purif. Technol.*, 2023, **311**, 123357, DOI: 10.1016/j.seppur.2023.123357.

24 H. L. Ho and M. S. Lee, A Review on the Recent Developments in the Dissolution of Rhodium and Iridium Metals from Spent Catalysts, *Miner. Process. Extr. Metall. Rev.*, 2024, 1–15, DOI: 10.1080/08827508.2024.2432667.

25 A. P. Paiva, F. V. Piedras, P. G. Rodrigues and C. A. Nogueira, Hydrometallurgical Recovery of Platinum-Group Metals from Spent Auto-Catalysts – Focus on Leaching and Solvent Extraction, *Sep. Purif. Technol.*, 2022, **286**, 120474, DOI: 10.1016/j.seppur.2022.120474.

26 M. L. Grilli, A. E. Slobozeanu, C. Larosa, D. Paneva, I. Yakoumis and Z. Cherkezova-Zheleva, Platinum Group Metals: Green Recovery from Spent Auto-Catalysts and Reuse in New Catalysts—A Review, *Crystals*, 2023, **13**(4), 550, DOI: 10.3390/cryst13040550.

27 Y. Ding, H. Zheng, J. Li, S. Zhang, B. Liu, C. Ekberg and Z. Jian, Recovery of Platinum from Spent Petroleum Catalysts: Optimization Using Response Surface Methodology, *Metals*, 2019, **9**(3), 354, DOI: 10.3390/met9030354.

28 A. J. Bard, R. Parsons and J. Jordan, *Standard Potentials in Aqueous Solution*, Marcel Dekker, Inc., New York, NY: United States, 1985, DOI: 10.1201/9780203738764.

29 M. H. H. Mahmoud, Leaching Platinum-Group Metals in a Sulfuric Acid/Chloride Solution, *JOM*, 2003, **55**(4), 37–40, DOI: 10.1007/s11837-003-0086-y.

30 J. Spooren and T. Abo Atia, Combined Microwave Assisted Roasting and Leaching to Recover Platinum Group Metals from Spent Automotive Catalysts, *Miner. Eng.*, 2020, **146**, 106153, DOI: 10.1016/j.mineng.2019.106153.

31 T. Suoranta, O. Zugazua, M. Niemelä and P. Perämäki, Recovery of Palladium, Platinum, Rhodium and Ruthenium from Catalyst Materials Using Microwave-Assisted Leaching and Cloud Point Extraction, *Hydrometallurgy*, 2015, **154**, 56–62, DOI: 10.1016/j.hydromet.2015.03.014.

32 Y. Zhao, N. M. Vargas-Barbosa, E. A. Hernandez-Pagan and T. E. Mallouk, Anodic Deposition of Colloidal Iridium Oxide Thin Films from Hexahydroxyiridate(IV) Solutions, *Small*, 2011, **7**(14), 2087–2093, DOI: 10.1002/smll.201100485.

33 Y. Zhao, N. M. Vargas-Barbosa, M. E. Strayer, N. S. McCool, M.-E. Pandelia, T. P. Saunders, J. R. Swierk, J. F. Callejas, L. Jensen and T. E. Mallouk, Understanding the Effect of Monomeric Iridium (III/IV) Aquo Complexes on the Photoelectrochemistry of $IrO_x \cdot nH_2O$-Catalyzed Water-Splitting Systems, *J. Am. Chem. Soc.*, 2015, **137**(27), 8749–8757, DOI: 10.1021/jacs.5b03470.

34 C. Massué, V. Pfeifer, M. van Gastel, J. Noack, G. Algara-Siller, S. Cap and R. Schlögl, Reactive Electrophilic O^{I-} Species Evidenced in High-Performance Iridium Oxohydroxide Water Oxidation Electrocatalysts, *ChemSusChem*, 2017, **10**(23), 4786–4798, DOI: 10.1002/cssc.201701291.

35 N. Papaiconomou, I. Billard and E. Chainet, Extraction of Iridium(iv) from Aqueous Solutions Using Hydrophilic/Hydrophobic Ionic Liquids, *RSC Adv.*, 2014, **4**(89), 48260–48266, DOI: 10.1039/C4RA06991A.

36 M. Kazemi, M. R. Hosseini, A. Zamaniyan and A. Ahmadi, Application of Cupric or Ferric Ions as Environmentally Benign Oxidants to the Chloride Leaching of Platinum from Spent Reforming Catalysts, *J. Environ. Manage.*, 2023, **337**, 117768, DOI: **10.1016/j.jenvman.2023.117768**.

37 W. H. Koppenol, D. M. Stanbury and P. L. Bounds, Electrode Potentials of Partially Reduced Oxygen Species, from Dioxygen to Water, *Free Radical Biol. Med.*, 2010, **49**(3), 317–322, DOI: **10.1016/j.freeradbiomed.2010.04.011**.

38 M. A. Bezerra, R. E. Santelli, E. P. Oliveira, L. S. Villar and L. A. Escaleira, Response Surface Methodology (RSM) as a Tool for Optimization in Analytical Chemistry, *Talanta*, 2008, **76**(5), 965–977, DOI: **10.1016/j.talanta.2008.05.019**.

39 J. G. Vos, Z. Liu, F. D. Speck, N. Perini, W. Fu, S. Cherevko and M. T. M. Koper, Selectivity Trends Between Oxygen Evolution and Chlorine Evolution on Iridium-Based Double Perovskites in Acidic Media, *ACS Catal.*, 2019, **9**(9), 8561–8574, DOI: **10.1021/acscatal.9b01159**.

40 V. R. Choudhary, C. Samanta and P. Jana, Decomposition and/or Hydrogenation of Hydrogen Peroxide over Pd/Al_2O_3 Catalyst in Aqueous Medium: Factors Affecting the Rate of H_2O_2 Destruction in Presence of Hydrogen, *Appl. Catal., A*, 2007, **332**(1), 70–78, DOI: **10.1016/j.apcata.2007.08.004**.

41 L.-K. Wu, K.-Y. Chen, S.-Y. Cheng, B.-S. Lee and C.-M. Shu, Thermal Decomposition of Hydrogen Peroxide in the Presence of Sulfuric Acid, *J. Therm. Anal. Calorim.*, 2008, **93**(1), 115–120, DOI: **10.1007/s10973-007-8829-6**.

42 B. V. Tilak, Kinetics of Chlorine Evolution—A Comparative Study, *J. Electrochem. Soc.*, 1979, **126**(8), 1343, DOI: **10.1149/1.2129274**.

43 D. W. Mckee, Catalytic Decomposition of Hydrogen Peroxide by Metals and Alloys of the Platinum Group, *J. Catal.*, 1969, **14**(4), 355–364, DOI: **10.1016/0021-9517(69)90326-1**.

44 D. Reig-i-Plessis, T. A. Johnson, K. Lu, Q. Chen, J. P. C. Ruff, M. H. Upton, T. J. Williams, S. Calder, H. D. Zhou, J. P. Clancy, A. A. Aczel and G. J. MacDougall, Structural, Electronic, and Magnetic Properties of Nearly Ideal J_{eff} =1/2 Iridium Halides, *Phys. Rev. Mater.*, 2020, **4**(12), 124407, DOI: **10.1103/PhysRevMaterials.4.124407**.

45 Y. V. Nelyubina, A. A. Korlyukov and K. A. Lyssenko, Experimental Charge Density Evidence for Pnicogen Bonding in a Crystal of Ammonium Chloride, *ChemPhysChem*, 2015, **16**(3), 676–681, DOI: **10.1002/cphc.201402673**.